

# Xmm-Newton Observations of the Diffuse X-ray Background

M. Galeazzi<sup>1</sup>, A. Gupta, K. Covey, and E. Ursino

*Physics Department, University of Miami, Coral Gables, FL 33155*

## ABSTRACT

We analyzed two XMM-Newton observations in the direction of the high density, high latitude, neutral hydrogen cloud MBM20 and of a nearby low density region that we called the Eridanus hole. The cloud MBM20 is at a distance evaluated between 100 and 200 pc from the Sun and its density is sufficiently high to shield about 75% of the foreground emission in the 3/4 keV energy band. The combination of the two observations makes possible the separation between foreground component, due to the Local Bubble and possibly charge exchange within the solar system, and the background one, due primary to the Galactic halo and unidentified point sources. The two observations are in good agreement with each other and with ROSAT observations of the same part of the sky and the  $O_{VII}$  and  $O_{VIII}$  intensities are  $O_{VII}=3.89\pm 0.56$  photons  $cm^{-2} s^{-1} sr^{-1}$ ,  $O_{VIII}=0.68\pm 0.24$  photons  $cm^{-2} s^{-1} sr^{-1}$  for MBM20 and  $O_{VII}=7.26 \pm 0.34$  photons  $cm^{-2} s^{-1} sr^{-1}$ ,  $O_{VIII}=1.63 \pm 0.17$  photons  $cm^{-2} s^{-1} sr^{-1}$  for the Eridanus hole.

The spectra are in agreement with a simple three component model, one unabsorbed and one absorbed plasma component, and a power law, due unresolved distant point sources. Assuming that the two plasma components are in thermal equilibrium we obtain a temperature of 0.096 keV for the foreground component and 0.197 keV for the background one. Assuming the foreground component is due solely to Local Bubble emission we obtain a lower and upper limit for the plasma density of  $0.0079 cm^{-3}$  and  $0.0095 cm^{-3}$  and limits of  $16,200 cm^{-3}K$  and  $19,500 cm^{-3}K$  for the plasma pressure, in good agreement with theoretical predictions. Similarly, assuming that the absorbed plasma component is due to Galactic halo emission, we obtain a plasma density ranging from  $0.0009 cm^{-3}$  to  $0.0016 cm^{-3}$ , and a pressure ranging from  $3.8 \times 10^3$  to  $6.7 \times 10^3 cm^{-3}K$ .

*Subject headings:* Local Bubble, Diffuse X-Ray background

---

<sup>1</sup>corresponding author, galeazzi@physics.miami.edu

## 1. Introduction

Optical and ultraviolet absorption line studies indicate that the Sun is located in a region of the interstellar medium of our Galaxy that is deficient in neutral matter, the Local Cavity (Cox et al. 1987; Frisch et al. 1983; Bochkarev 1987). Observations of the X-ray background at energies below 1 keV indicate that this cavity is largely filled with million degree plasma, the Local Bubble (LB), and it extends for distances of the order of 100 pc in most directions.

Fits to data obtained with proportional counters have indicated temperatures near one million degrees for the LB, if one compares the shape of the pulse height distribution to predictions of models with normal solar abundances and collisional equilibrium ionization structure of the plasma (Snowden et al. 1998). Higher resolution spectral data over the 150-300 eV range obtained near the galactic plane with a Bragg crystal spectrometer (Sanders et al. 2001) confirm the thermal nature of the LB X-ray emission, but indicate that the above model picture is a bit naïve. The data suggest that the LB plasma is not in equilibrium and the abundances are probably not solar.

High resolution observations of the diffuse background at high galactic latitude obtained by ASCA in the 500-1000 eV range using CCD detectors (Gendreau et al. 1995) and by the XQC sounding rocket experiment in the 50-2000 eV range using microcalorimeter detectors (McCammon et al. 2002) detect the existence of the O VII and O VIII lines, but cannot separate the LB emission from galactic halo and extragalactic components. A more recent observation of the neutral hydrogen cloud MBM12 performed with Chandra (Smith et al. 2005) is also not able to clarify the picture as it seems affected by charge exchange within the solar system. A cleaner observation of MBM12 and a blank field less than  $3^\circ$  away has recently been performed with Suzaku (Smith et al. 2006). The Suzaku observation does not seem to be affected by a strong contribution of charge exchange within the local system and the use of the second field of view helps in separating the local and distant components of the diffuse soft X-ray background.

## 2. Observations

For this analysis we used two 100 ks observations taken with the XMM-Newton satellite in the direction respectively of the high density, high latitude, neutral hydrogen cloud MBM20 (Observation ID : 0203900201) from 2004-08-23 to 2004-08-24 and of a nearby low density region, that we called the Eridanus hole (Observation ID : 0203900101) from 2004-08-09 to 2004-08-10. MBM20 is a high latitude star forming cloud which is probably located

within or at the edge of the Local Bubble. Its mass is  $84M_{\odot}$  and it is located at coordinates  $l=211^{\circ}23'53''.2$ ,  $b=-36^{\circ}32'41''.8$ , southwest of the Orion star forming complex. The most recent evaluation of the distance  $d$  of MBM20 is based on interstellar NaI D absorption lines (Hearty et al. 2000). The nearest star which showed interstellar NaI D absorption in the line of sight to MBM20 is HD29851, at a distance of  $161 \pm 21$  pc using Hipparcos distances for stars. The farthest star which did not show NaI D absorption lines is HIP21508 at  $112 \pm 15$  pc. The currently accepted distance to MBM20 is therefore  $112 \pm 15$  pc  $< d < 161 \pm 21$  pc. The Eridanus hole, at coordinates  $l=213^{\circ}25'52''.3$ ,  $b=-39^{\circ}5'26''.6$ , is a low neutral hydrogen column density region located about 2 degrees from the highest density part of MBM20.

We used the IRAS 100  $\mu\text{m}$  maps to evaluate the neutral hydrogen density in the two regions. The IRAS average brightness is  $13.34$  MJy  $\text{sr}^{-1}$ , and  $0.73$  MJy  $\text{sr}^{-1}$  for MBM20 and the Eridanus hole respectively. Using the "typical" high-latitude 100  $\mu\text{m}/N_{\text{H}}$  ratio of  $0.85 \times 10^{-20}$   $\text{cm}^2$  MJy  $\text{sr}^{-1}$  (Boulanger & Perault 1988) the evaluated neutral hydrogen densities are  $1.59 \times 10^{21} \text{cm}^{-2}$  for MBM20 and  $0.86 \times 10^{20} \text{cm}^{-2}$  for the Eridanus hole.

A detailed analysis of the shadow effect of MBM20 and the Eridanus hole is reported in section 4. However a simple procedure to estimate the effect in the 0.5-1 keV energy range is by assuming that the background X-ray flux is due to thermal emission with  $\log_{10}(kT) = 6.2$ . We can then use the cross section calculated for the ROSAT 3/4 keV band as a good approximation of the cross section in the energy interval 0.5-1 keV. Using the calculation of Snowden et al. (1994) the cross section is approximately  $0.8 \times 10^{-21}$   $\text{cm}^2$  for MBM20 and  $1.0 \times 10^{-21}$   $\text{cm}^2$  for the Eridanus hole. Using the expression for photoelectric absorption  $M(E) = \exp(-N_{\text{H}}\sigma(E))$ , where  $\sigma(E)$  is the photoelectric cross section, we therefore get that approximately 75% of the background in the MBM20 pointing is absorbed, while only about 8% of it is absorbed in the Eridanus hole pointing. The combination of the two observations therefore allows good separation between foreground and background emission. Since MBM20 may be outside the LB or fairly close to the LB wall in that direction (Sfeir et al. 1999), the separation should be roughly equivalent to a separation between Local Bubble and Galactic Halo emissions.

### 3. Data Analysis

Data from the full XMM-Newton field of view (approximately  $30'$ ) were used in the analysis. The raw data were processed using the Standard Analysis Software (SAS)<sup>1</sup>. We looked at the MOS1, MOS2 and PN detector data and after a preliminary analysis we decided

---

<sup>1</sup><http://xmm.vilspa.esa.es/sas/>

that the background component in the MOS1 and MOS2 was too large and difficult to subtract in comparison to that of the PN detector. Despite the slightly better energy resolution of the MOS detectors we therefore decided to limit our analysis to the PN detector. We selected events with pattern 0-4 (single+double) and flag equal to zero, to exclude bad pixels and CCD gaps. To remove the CCD pixels affected by proton flares and events above threshold, we generated light curves and removed all time intervals with a count rate greater than 20 counts  $\text{s}^{-1}$ . We found 15 point sources for MBM20 and 33 point sources for the Eridanus hole using our own code that iteratively identifies regions with count rate  $3\sigma$  above the average observation count rate. For each identified source we excluded a region of  $1'$  radius around the source location (see Figs. 1 and 2). After removal of bad pixels and point sources, the active field of view is  $5.1 \times 10^{-5}$  sr for the MBM20 observation and  $4.9 \times 10^{-5}$  sr for the Eridanus hole one.

### 3.1. Background Removal

During the data analysis, we tried several procedures to properly evaluate the background. In the end we found that the relatively simple procedure reported here worked as well as any more complex one we tried. To account for systematic problems related to the background removal, a systematic error is included in our results. The systematic error is evaluated by taking into account the spread in the results when different background removal procedures were used.

The non-cosmic background was modeled using a method similar to that proposed in Kuntz and Snowden (2004) and Read and Ponman (2003). The nominal non-cosmic background, which is dominated by the quiescent, high energy particle induced background, is modeled using closed-filter data (Read & Ponman 2003). To scale the closed-filter data to our observations, a spectrum of the closed filter dataset was created using the same procedure and filtering as was used to produce our spectra. The closed filter spectrum was then normalized using the counts in the Cu lines. We found that this procedure is very efficient at removing the "internal" background of the detector.

To remove the remaining ("external") background, we first subtracted from the spectra the well characterized power law component due to unidentified point sources (using the data from McCammon et al. 2002). Since this is the only significant component of the Diffuse X-ray Background (DXB) at high energy, the remaining spectrum at energies above about 2 keV is completely due to the external detector background. As can be seen in Fig. 3, above 2 keV this background is well described by a single exponential function of the energy both for MBM20 and the Eridanus hole data. To remove the external background from the region

of our interest (0.5-1 keV), we then fit this exponential background above 2 keV and extend it, with the same parameters, in the region of interest. We then go back to our original data (after the internal background subtraction) and remove the exponential background to obtain the clean spectra. As will be discussed in the result section, the accuracy of the procedure has been confirmed by the good agreement between our data and ROSAT observations in the same directions. We also verified that the fitting range for the exponential background is not critical and small changes in the final result have been included in the systematic error.

#### 4. Analysis

A simple picture of the DXB nature points to the existence of three separate components, a local bubble component, modeled as an unabsorbed plasma thermal emission, a hotter galactic halo emission, modeled as a plasma thermal component absorbed by the gas in the galactic disk, and an unresolved extragalactic sources component (primarily AGNs), modeled as an absorbed power law. While high resolution observations in the 1/4 keV energy band have shown that this picture is too naïve (Sanders et al.2001, McCammon et al. 2002), considering the energy resolution of the PN detector, we decided to use it as a starting point for our analysis. We used the XSPEC analysis package (Arnaud & Dormer 2002) to fit both spectra, in the energy range 0.4-2 keV, using a three component model. For plasma thermal emission the APEC<sup>2</sup> model has been used. The unresolved extragalactic source component is a simple photon power law given as  $A(E)=KE^{-\alpha}$  where  $\alpha$  is the photon index of the power law and E is energy in keV. In the fits, the neutral hydrogen density for the absorbed components was fixed to the average value obtained from the analysis of the IRAS-100 data ( $15.9 \times 10^{20} \text{ cm}^{-2}$  and  $0.86 \times 10^{20} \text{ cm}^{-2}$  for MBM20 and the Eridanus hole respectively), while all the other parameter were left free. For easy comparison with other investigations, the solar metal relative abundance of Anders et al. (1989) has been chosen for the analysis. Due to a strong correlation between total metallicity and luminosity in the thermal components, we also decided to repeat the fits fixing the total metallicity to 1 (in solar units). The changes in the O VII and O VIII emission line fluxes due to different fitting procedures have been incorporate in the systematic error. In Table 1 we report the best fit parameters for the MBM20 and Eridanus hole datasets respectively, using a three components model, with fixed and free metal abundances. In view of a reasonably good agreement between the fits of MBM20 and the Eridanus hole, we decided to fit both datasets at once, with a single set of parameters, except, of course, for the neutral hydrogen column density. The results are reported in Table 2, and the fits are shown in Fig. 4. In the Figure the O VII triplet at 561 eV,

---

<sup>2</sup><http://hea-www.harvard.edu/APEC/>

569 eV, and 574 eV is clearly visible in both observations, while the O VIII line at 654 eV is barely visible in the Eridanus hole dataset and within the statistical uncertainty in the MBM20 dataset. In the table, the parameters obtained by McCammon et al. (2002) are also shown for comparison. The best fit results are in good agreement with those in McCammon et al. (2002), and the model fits very well the experimental data. To verify the robustness of the fit results, we repeated the procedure for different energy intervals, but we didn't find any significant change in fit parameters or reduced chi square. We also decided to repeat the fits using different solar elemental abundances and an elemental abundance depleted in heavy elements (Savage & Sembach 1996). The results are reported in Table 3 together with the oxygen metal abundance for the different metallicity models. Our result show that the choice of the metallicity model does not significantly affect the flux of the O VII and O VIII flux and small changes are included in the systematic error.

To verify the accuracy of our results, we compared them with data from the ROSAT All Sky Survey (RASS) in the same directions. For the comparison we extracted RASS data in the bands R1-R7 (Snowden et al. 1998) and scaled to the same FOV of our XMM-Newton datasets both for MBM20 and the Eridanus Hole. We then performed a global fit of the four datasets at once with a single set of parameters. The fit results are reported in Table 4 and the data are shown in Fig. 5. The inclusion of the RASS data does not significantly change the best fit parameters, which are compatible with the previous ones using only XMM-Newton data. Moreover, the value of  $\chi^2$  is not significantly different, confirming the good agreement between our results and the RASS data and the reliability of our analysis procedure.

Having confirmed the reliability of our fit results, we used them to obtain the O VII and O VIII flux, which are reported in Table 6. In the table, the flux obtained by other investigations of the LB emission are also reported. As pointed out before, the error on the line flux is a combination of a purely statistical error and a systematic error that accounts for changes due to different analysis and background subtraction procedures.

Combining the MBM20 and Eridanus hole data we can evaluate O VII and O VIII emission of the foreground (LB) and background (galactic halo) components. Using the expression for cross section per hydrogen atom derived by Morrison and McCammon (Morrison & McCammon 1983),  $\sigma(E)=(C_0 +C_1E+C_2E^2)E^{-3}\times 10^{-24} \text{ cm}^{-2}$ , where  $C_0$ ,  $C_1$  and  $C_2$  are coefficient of analitical fit to Cross Section (given in their Table 2.), we find that MBM20 absorbs about 75% of the background O VII emission and about 61% of the background O VIII emission, while the Eridanus hole absorbs about 8% of the background O VII emission and about 5% of the background O VIII emission. Combining these data with our results, we evaluate the intensities of O VII and O VIII for the foreground component (LB) as  $2.63 \pm 0.78 \text{ photons cm}^{-2} \text{ s}^{-1} \text{ sr}^{-1}$

and  $0.03 \pm 0.43$  photons  $\text{cm}^{-2} \text{s}^{-1} \text{sr}^{-1}$  respectively, and for the background component as  $5.03 \pm 0.98$  photons  $\text{cm}^{-2} \text{s}^{-1} \text{sr}^{-1}$  and  $1.68 \pm 0.53$  photons  $\text{cm}^{-2} \text{s}^{-1} \text{sr}^{-1}$ .

Assuming that hydrogen and helium are fully ionized, we can also use the results of our fits to evaluate the electron density, given by  $n_e^2 = \frac{1.225 * EM}{R}$ , where  $R$  is the spatial extension of the plasma region, corresponding to the smallest between the radius of the Local Bubble and the distance of MBM20 and EM is the Emission Measure. Since the two distances are expected to be comparable, we used the MBM20 distance to evaluate the electron density, obtaining a lower limit of  $0.0079 \text{ cm}^{-3}$  and an upper limit of  $0.0095 \text{ cm}^{-3}$  using the result from the collisional equilibrium plasma model with solar elemental abundances. From the electron density we can also evaluate the thermal pressure of the plasma  $P_{\text{th}} = 1.92 n_e T$ . The upper and lower limits for the thermal pressure, are  $16,200 \text{ cm}^{-3} K$  and  $19,500 \text{ cm}^{-3} K$  respectively. Our results are comparable to the models of LB as discussed by Smith and Cox (Smith et al. 2001), using a series of two or three spatially coincident supernova explosions. They predicted for an isothermal gas in collisional equilibrium, thermal pressure of  $p/k = 2.4, 1.8, \text{ or } 1.0 \times 10^4 \text{ cm}^{-3} K$  and  $R = 87, 103, \text{ or } 102 \text{ pc}$  at temperature  $T = 1.15, 1.8, \text{ or } 1.5 \times 10^6 K$ . Our result is also in agreement with a recent observation of the neutral hydrogen cloud MBM12 performed with Suzaku (Smith et al. 2006). Smith et al. (2006) obtained an emission measure of  $0.02, 0.0075, \text{ or } 0.0023 \text{ cm}^{-6} \text{ pc}$ , electron densities of  $0.014, 0.0087, \text{ or } 0.0048 \text{ cm}^{-3}$ , and thermal pressure of  $p/k = 3.0, 2.2, \text{ or } 1.7 \times 10^4 \text{ cm}^{-3} K$  at temperature of  $T = 1.0, 1.2, \text{ or } 1.7 \times 10^6 K$  respectively for the LB.

We used the same procedure to evaluate the thermal pressure of the galactic halo. Using a thickness  $D$  for the Galactic Halo ranging from  $1.6 \text{ kpc}$  to  $4.9 \text{ kpc}$  (Shull & Slavin 1993), we get electron densities of  $0.0016 \text{ cm}^{-3}, 0.0009 \text{ cm}^{-3}, \text{ or } 0.0011 \text{ cm}^{-3}$ , and pressures of  $p/k = 6.7, 3.8, \text{ and } 4.7 \times 10^3 \text{ cm}^{-3} K$  for  $D = 1.6, 4.9, \text{ and } 3.25 \text{ kpc}$  respectively.

Despite the conclusions of higher resolution investigations (Sanders et al. 2001, McCammon et al. 2002), our results show that the simple three components model used is accurate enough for the interpretation of the data, due to the limited energy resolution of the XMM-Newton PN detector. This precludes any significant deeper analysis of the data with more complex models. Nevertheless, we decided to probe the hypothesis that the data are not in equilibrium. For this purpose, we used the non equilibrium plasma model GNEI (Borkowski 2000), a Plane-parallel Shock Model characterized by a constant postshock electron temperature and by its ionization age. The result of the fit is reported in table 5. Assuming a constant electron density within the Local Bubble, using the data from Table 4 we obtain a lower limit on the electron density of  $0.01 \text{ cm}^{-3}$  and an upper limit of  $0.012 \text{ cm}^{-3}$ . From the ionization timescale, defined as the product of the remnant's age and electron number density, we can also evaluate the age of the LB as  $\lesssim 0.6 \text{ Myr}$ , which is

quiet less in comparison to most acceptable models of the LB at temperature of  $1.2 \times 10^6$  K. For example, Smith and Cox (Smith et al. 2001) in their model of the LB as a series of supernovae, obtained age of LB between 2.6-6.0 Myr. Shelton (Shelton et al. 2003) from the O VI resonance line emission originating in the Local Bubble using the Far-Ultraviolet Spectroscopic Explorer (FUSE), obtained a lower limit for the age of LB of 2 Myr.

Our results are also significantly different from what has been found in a Chandra observation of the neutral hydrogen cloud MBM12, where a very strong O VIII emission line was observed (Smith et al. 2005) and the simple three component model could not be used successfully. The authors of the MBM12 paper concluded that their measurement was probably affected by particularly strong emission due to charge exchange within the solar system. Assuming that the higher O VIII emission is, in fact, a signature of charge exchange within the solar system, we can conclude that such contamination is not significant in our data.

We investigated the possibility that the discrepancy with the MBM12 data could be purely due to a different pointing directions. We used the maps of the expected X-ray emission due to charge exchange with interstellar neutrals and geocoronal hydrogen within the solar system generated by Robertson and Cravens (2003) to evaluate the expected contribution in the direction of MBM20 and MBM12. From the X-ray map at the time of the ROSAT 1990-1991 sky survey, we find that the X-ray intensity due to charge exchange in MBM12 is  $4\text{-}5 \text{ keV cm}^{-2} \text{ s}^{-1} \text{ sr}^{-1}$ , while in the MBM20 direction is  $3\text{-}4 \text{ keV cm}^{-2} \text{ s}^{-1} \text{ sr}^{-1}$ . While, in fact, the emission in the direction of MBM20 is expected to be smaller, the difference should be less than 30%, which cannot explain the difference between our results and those of Smith et al. (2005). We should therefore conclude that either the high O VIII emission in the MBM12 observation is of different nature, or it is affected by a strong transient component which is not present in the MBM20 and Eridanus hole data.

## 5. Conclusions

In studying the Diffuse X-ray Background (DXB), a challenging task is the separation between the different components contributing to it. This is particularly difficult due to the low DXB flux compared to the relatively high detector background. The contemporary study of a high latitude, high density cloud and a low density region nearby has proven an effective tool for the separation of foreground and background components. In our investigation we found a simple, efficient method to evaluate the detector background and the comparison of the two pointing gives us good separation between the two main DXB plasma components, i.e., Local Bubble and Galactic halo. The results are consistent with a simple

three components model of the DXB: an unabsorbed plasma component with temperature of 0.096 keV, an absorbed plasma component with temperature of 0.197 keV, and a power law, due to unresolved distant point sources.

Assuming the foreground component is due solely to Local Bubble emission we obtain a lower and upper limit for the plasma density of  $0.0079 \text{ cm}^{-3}$  and  $0.0095 \text{ cm}^{-3}$  and  $16,200 \text{ cm}^{-3}K$  and  $19,500 \text{ cm}^{-3}K$  for the plasma pressure, in agreement with theoretical predictions (e.g., (Smith et al. 2001)) and similar observations (e.g., (?)). Similarly, assuming that the absorbed plasma component is due to Galactic halo emission, we obtain a plasma density ranging from  $0.0009 \text{ cm}^{-3}$  to  $0.0016 \text{ cm}^{-3}$ , and a pressure ranging from  $3.8 \times 10^3$  to  $6.7 \times 10^3 \text{ cm}^{-3}K$ .

We also tested the possibility that the plasma is not in equilibrium using a Plane-parallel Shock Model (Borkowski 2000). However, while we obtained good fit and the electron density of ranges from  $0.01 \text{ cm}^{-3}$  to  $0.012 \text{ cm}^{-3}$ , we derived a value for the age of the LB of  $\leq 0.6 \text{ Myr}$ , which is quiet less in comparison to most acceptable models.

We would like to thank Kip Kuntz for the useful discussion about XMM-Newton background removal and for providing us preprints of his publication on the subject. We would also like to thank Wilt Sanders and Dan McCammon for the useful discussion and suggestions and the referee for the useful suggestions. The investigation was supported in part by NASA grant #NNG05GA84G.

## REFERENCES

- Anders,E., et al., 1989, *Geochimica et Cosmochimica Acta*,53, 197
- Anders, E. & Ebihara, ., et al. 1982,*Geochimica et Cosmochimica Acta*,46, 2363
- Arnaud, K. & Dormer, B. 2002, XSPEC:An X-Ray Spectral Fitting package,User’s Guide for version 11.2.x, HEASARC, Exploration of the Universe Division, NASA/GSFC, Greenbelt, MD 20771, <http://heasarc.gsfc.nasa.gov/docs/xanadu/xspec/manual/manual.html>
- Bochkarev, N. G. et al. 1987, *Soviet Ast.*, 31, 20
- Borkowski, K. J. et al. 2000, *ApJ*, 548, 820
- Boulanger, F., and Perault, M. 1988, *ApJ*, 330, 964

- Cox, D. P., et al. 1987, ARA&A, 25,303
- Frisch, P. L., et al. 1983, ApJ,271, 59
- Gendreau, K. C., et al. 1995, PASJ, 47, L5
- Grevese, N. & Sauval, A. J., et al. 1998, Space Science Reviews 85, 161
- Hearty, T., et al. 2000, A&A, 357, 681
- Lodders, K.,et al. 2003,ApJ, 591, 1220
- McCammon, D., et al. 2002, ApJ, 576, 188
- Morrison, R. & McCammon, D., et al. 1983, ApJ, 270, 119
- Read, A. M. & Ponman, T. J. 2003, A&A, 409,395
- Robertson, I. P. & Cravens, T. E. 2003, J. Geophys. Res., 108, A10, LIS 6-1
- Sanders, W. T., et al. 2001, ApJ, 554, 694
- Savage, B. D.& Sembach, K. R., et al. 1996, ARAA, 34,279
- Sfeir, D. M., et al. 1999, A&A, 346, 785
- Shelton, R. L., et al. 2003, ApJ, 589, 261
- Shull, J. M. & Slavin, J. D.,et al. 1993, ApJ, 427, 784
- Smith, R. K., et al., 2001, ApJSupplement Series, 134:283-309
- Smith, R. K., et al., 2005, ApJ, 623, 225
- Smith, R. K., et al., 2006, PAST. 1
- Snowden, S. L., et al., 1994, ApJ, 424, 714
- Snowden, S. L., et al., 1998, ApJ, 493, 715

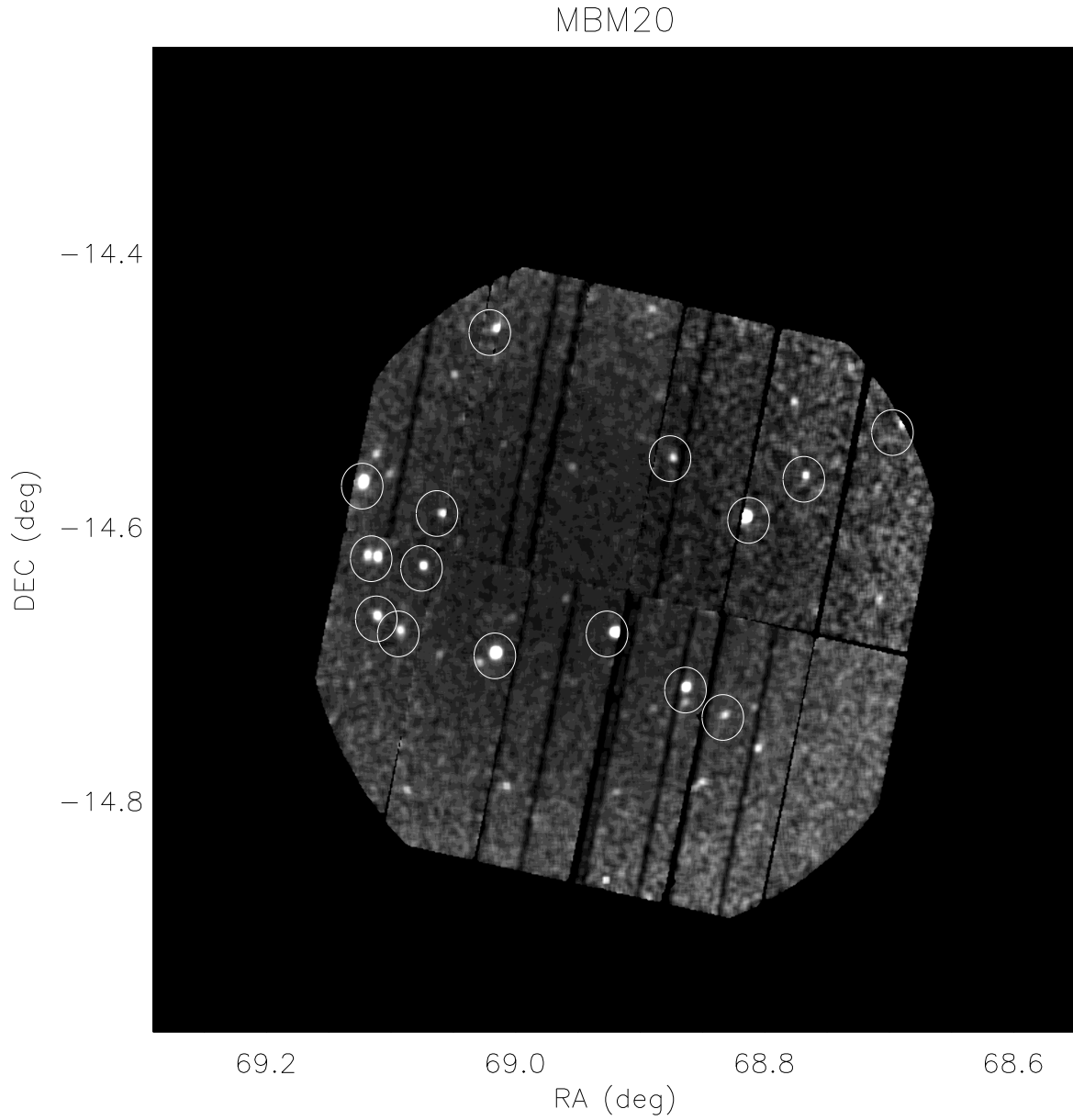


Fig. 1.— EPIC-PN image of MBM20 in the energy range 0.4-2 keV. The white circles represent the area around identified point sources that has been excluded in the analysis.

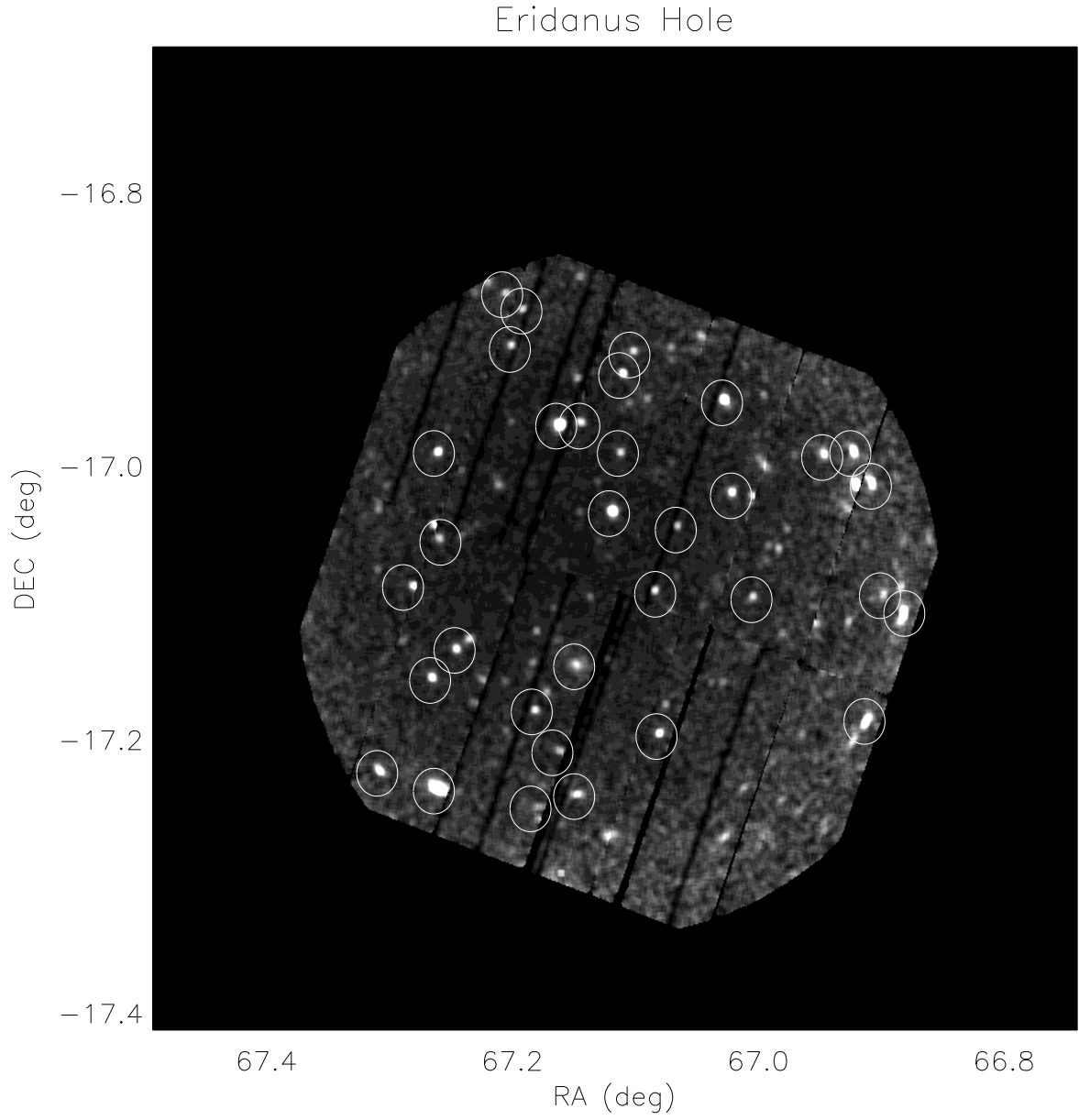


Fig. 2.— EPIC-PN image of the Eridanus Hole in the energy range 0.4-2 keV. The white circles represent the area around identified point sources that has been excluded in the analysis.

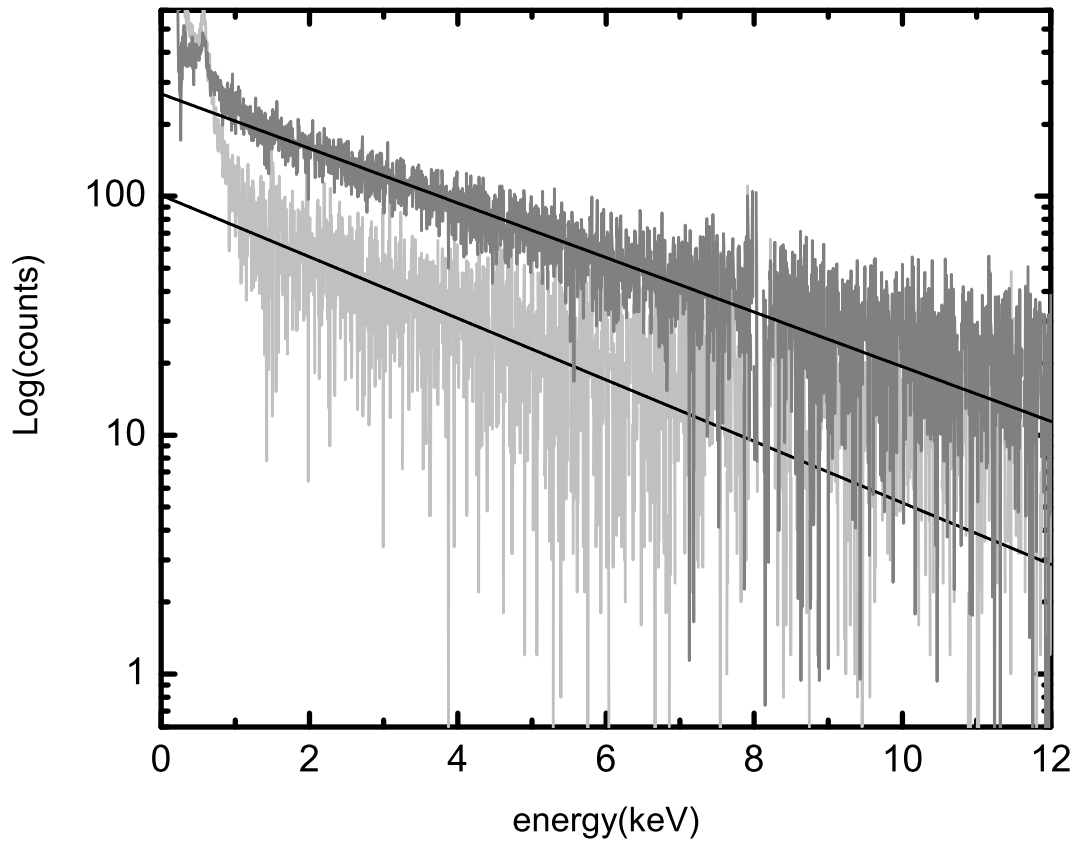


Fig. 3.— Energy spectrum from the MBM20 (dark grey line) and Eridanus hole (grey line) observations after subtracting the internal background and the unidentified sources component. The events above about 2 keV are completely due to external detector background and can be well characterized by a simple exponential function of the energy.

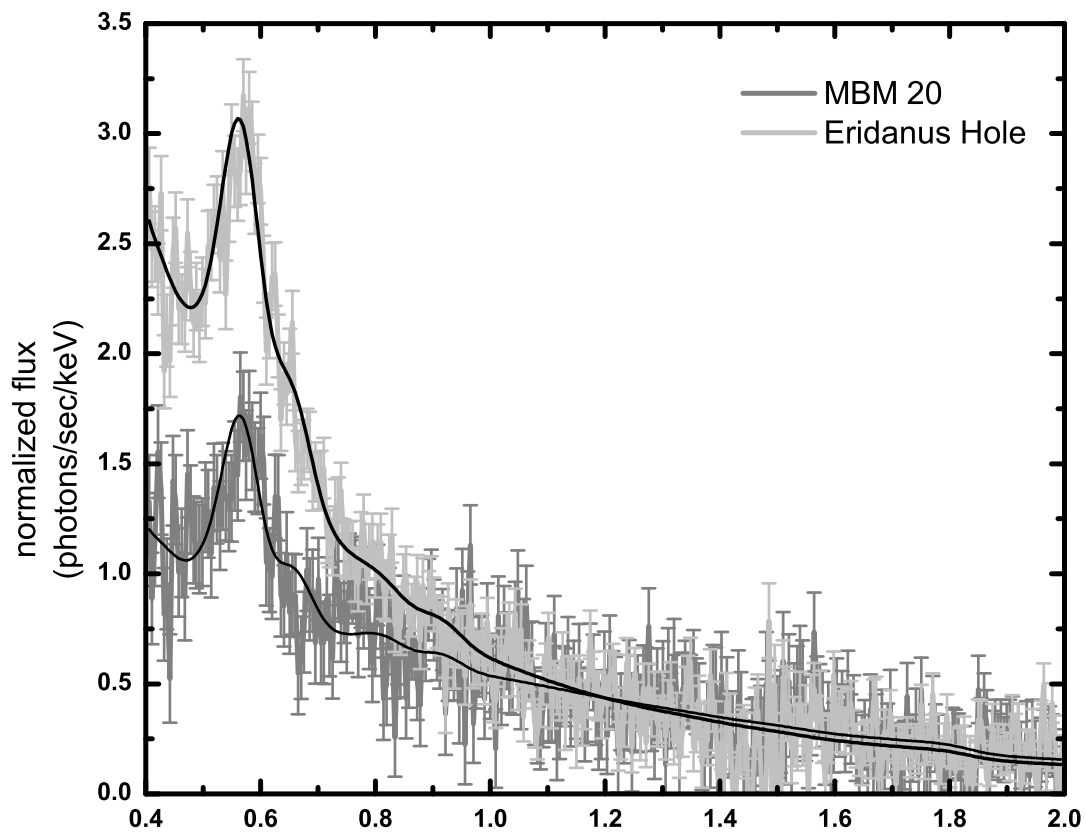


Fig. 4.— Global fit for MBM20 and Eridanus hole data. The datapoints represent the experimental data, the black lines the best fits.

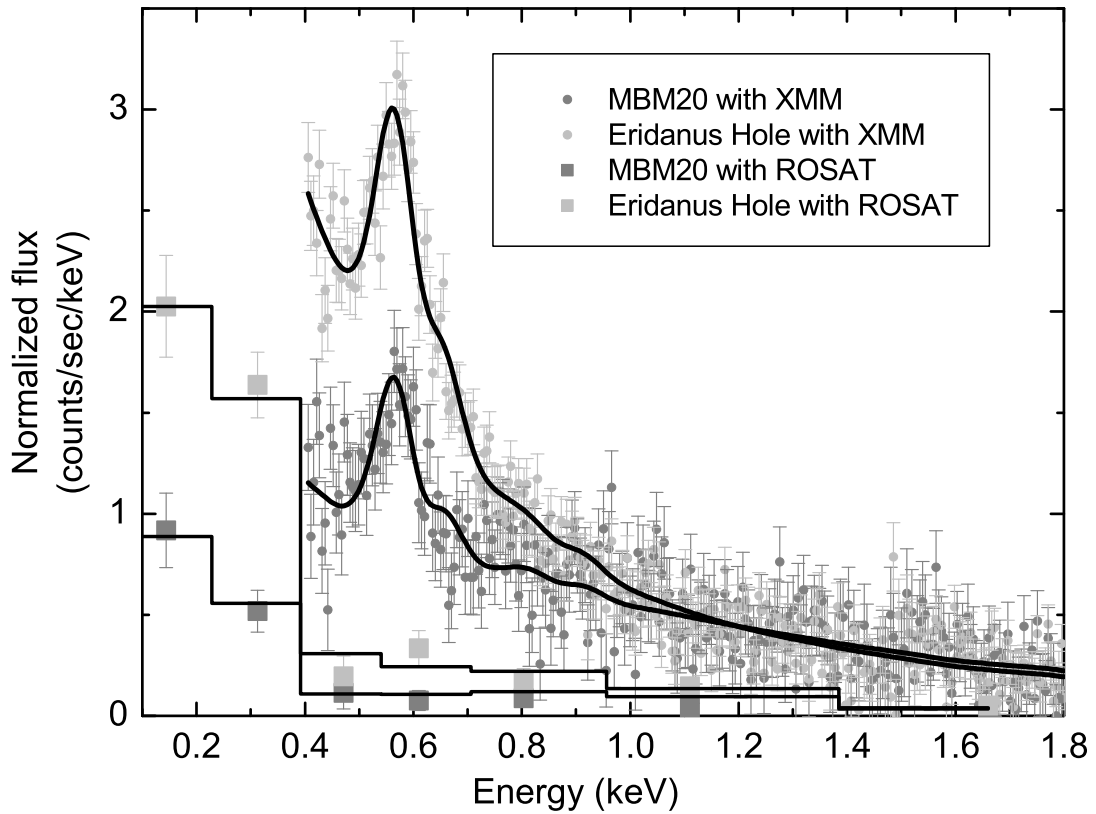


Fig. 5.— Global fit of MBM20 (dark grey) and the Eridanus hole (light grey) using data from our investigation (circles) and the RASS (squares). The black lines represent the best fits.

Table 1. Best fit parameters for the MBM20 and Eridanus hole datasets respectively, using a three components model. The terms "Free" and "Frozen" refers to Free abundance and Frozen abundance.

		MBM20		Eridanus hole	
	Units	Free	Frozen	Free	Frozen
<b>Unabsorbed plasma component:</b>					
Temperature	keV	0.114	0.099	0.097	0.094
	$10^6$ K	1.33	1.15	1.13	1.09
Abundance	Solar Units	0.92	1	0.54	1
Emission Measure	$\text{cm}^{-6}$ pc	0.0051	0.0082	0.0213	0.013
<b>Absorbed plasma component:</b>					
nH	$10^{22}$ $\text{cm}^2$	0.159	0.159	0.0086	0.0086
Temperature	keV	0.21	0.242	0.211	0.205
	$10^6$ K	2.44	2.81	2.45	2.38
Abundance	Solar Units	0.667	1	0.208	1
Emission Measure	$\text{cm}^{-6}$ pc	0.0009	0.0014	0.0107	0.0248
<b>Absorbed power law:</b>					
Photon Index		2.48	2.32	1.93	1.99
Normalization	ph $\text{keV}^{-1}$ $\text{s}^{-1}$ $\text{cm}^{-2}$	15.7	14.86	12.7	12.6
<b>Reduced Chi square</b>		0.93	0.93	1.5	1.5
Degrees of freedom		315	317	315	317

Table 2. Model Parameters for global fit of MBM20 and Eridanus hole data. In the neutral hydrogen density row, we first list the column density toward MBM20 and then the column density toward the Eridanus Hole in the “Free Abundance” and “Frozen Abundance” columns.

	Units	Free Abundance	Frozen Abundance	McCammon
<b>Unabsorbed plasma component:</b>				
Temperature	keV	0.104	0.095	0.099
	$10^6$ K	1.21	1.11	1.15
Abundance	Solar Units	0.39	1	1
Emission Measure	$\text{cm}^{-6}$ pc	0.034	0.0082	0.0088
<b>Absorbed plasma component:</b>				
nH	$10^{22}$ $\text{cm}^2$	0.159/0.0086	0.159/0.0086	
Temperature	keV	0.196	0.191	0.225
	$10^6$ K	2.19	2.27	2.62
Abundance	Solar Units	0.453	1	1
Emission Measure	$\text{cm}^{-6}$ pc	0.0075	0.0034	0.0037
<b>Absorbed power law:</b>				
Photon Index		2.12	2.2	1.52
Normalization	ph $\text{keV}^{-1}$ $\text{s}^{-1}$ $\text{cm}^{-2}$	14.8	14.8	12.3
<b>Reduced Chi square</b>				
Degrees of freedom		638	640	

Table 3. Model Parameters for global fit of MBM20 and Eridanus hole data using different abundance tables. The oxygen abundance is given relative to hydrogen.

	Units	Model <sup>a</sup>	Model <sup>b</sup>	Model <sup>c</sup>	Model <sup>d</sup>	Model <sup>e</sup>
<b>Oxygen abundance</b>	$10^{-4}$	8.51	7.39	6.76	4.9	3.02
<b>Unabsorbed plasma component:</b>						
Temperature	keV	0.095	0.1	0.096	0.1	0.12
Emission Measure	$\text{cm}^{-6} \text{ pc}$	0.0082	0.0072	0.0093	0.0108	0.0075
<b>Absorbed plasma component:</b>						
Temperature	keV	0.191	0.191	0.191	0.191	0.194
Emission Measure	$\text{cm}^{-6} \text{ pc}$	0.0034	0.004	0.0043	0.0061	0.0090
<b>Absorbed power law:</b>						
Photon Index		2.2	2.2	2.2	2.2	2.2
Normalization	$\text{ph keV}^{-1} \text{ s}^{-1} \text{ cm}^{-2}$	14.8	14.8	14.7	14.7	15.2
<b>Reduced Chi square</b>		1.2	1.2	1.2	1.2	1.3
Degrees of freedom		640	640	640	640	640

<sup>a</sup>Solar elemental abundance table of (Anders et al. 1989)

<sup>b</sup>Solar elemental abundance table of (Anders & Ebihara 1982)

<sup>c</sup>Solar elemental abundance table of (Grevese & Sauval 1998)

<sup>d</sup>Solar elemental abundance table of (Lodders et al. 2003)

<sup>e</sup>Depleted elemental abundance table of (Savage & Sembach 1996) for clouds  $\zeta$  towards Ophiuchi (their table 5)

Table 4. Model Parameters for global fit of MBM20 and Eridanus hole data from XMM-Newton and Rosat with cosmic elemental abundances.

	Units	Model Parameters
<b>Unabsorbed Non Equilibrium plasma component:</b>		
Temperature	keV	0.096
	$10^6$ K	1.11
Emission Measure	$\text{cm}^{-6}$ pc	0.0078
<b>Absorbed plasma component:</b>		
nH	$10^{22}$ $\text{cm}^2$	0.159/0.0086
Temperature	keV	0.191
	$10^6$ K	2.27
Emission Measure	$\text{cm}^{-6}$ pc	0.0035
<b>Absorbed power law:</b>		
Photon Index		2.2
Normalization	ph $\text{keV}^{-1}$ $\text{s}^{-1}$ $\text{cm}^{-2}$	14.8
<b>Reduced Chi square</b>		
Degrees of freedom		654

Table 5. Non Equilibrium Plasma Model Parameters for global fit of MBM20 and Eridanus hole data with cosmic elemental abundances.

	Units	Model Parameters
<b>Unabsorbed Non Equilibrium plasma component:</b>		
Temperature	keV	0.086
	$10^6$ K	0.99
Ionization timescale	$10^{12}$ s $\text{cm}^{-3}$	0.18
averaged plasma temperature	keV	.16
Emission Measure	$\text{cm}^{-6}$ pc	0.014
<b>Absorbed plasma component:</b>		
nH	$10^{22}$ $\text{cm}^2$	0.159/0.0086
Temperature	keV	0.186
	$10^6$ K	2.17
Emission Measure	$\text{cm}^{-6}$ pc	0.0036
<b>Absorbed power law:</b>		
Photon Index		2.2
Normalization	ph $\text{keV}^{-1}$ $\text{s}^{-1}$ $\text{cm}^{-2}$	14.1
<b>Reduced Chi square</b>		
Degrees of freedom		638

Table 6. O<sub>VII</sub> and O<sub>VIII</sub> intensities compared with previous estimates

Experiment	N <sub>H</sub> (10 <sup>20</sup> atoms cm <sup>-2</sup> )	O <sub>VII</sub> (ph s <sup>-1</sup> cm <sup>-2</sup> sr <sup>-1</sup> )	O <sub>VIII</sub> (ph s <sup>-1</sup> cm <sup>-2</sup> sr <sup>-1</sup> )
MBM20	15.9	3.89 ± 0.56	0.68 ± 0.24
Eridanus hole	0.86	7.26 ± 0.34	1.63 ± 0.17
Smith(2005)	40	1.79 ± 0.55	2.34 ± 0.36
Smith(2006)	40	3.34 ± 0.26	0.24 ± 0.1
Gendreau(1995)	6	2.3 ± 0.3	0.6 ± 0.15
McCammon(2002)	1.8	4.8 ± 0.8	1.6 ± 0.4